ARL-TR-9093 ● OCT 2020

DEVCOM ARMY RESEARCH LABORATORY

The Potential Impact of Assimilating Satellite-Derived Atmospheric Motion Vectors in Numerical Weather Prediction Modeling for Nowcasting

by Robert E Dumais Jr

ARL-TR-9093 ● OCT 2020

The Potential Impact of Assimilating Satellite-Derived Atmospheric Motion Vectors in Numerical Weather Prediction Modeling for Nowcasting

Robert E Dumais Jr
Computational and Information Sciences Directorate, CCDC Army Research Laboratory

REPORT DOCUMENTATION PAGE						*Form Approved* *OMB No. 0704-0188*
Public reporting burden for this collection of information is estimated to average 1 hour per response, including the time for reviewing instructions, searching existing data sources, gathering and maintaining the data needed, and completing and reviewing the collection information. Send comments regarding this burden estimate or any other aspect of this collection of information, including suggestions for reducing the burden, to Department of Defense, Washington Headquarters Services, Directorate for Information Operations and Reports (0704-0188), 1215 Jefferson Davis Highway, Suite 1204, Arlington, VA 22202-4302. Respondents should be aware that notwithstanding any other provision of law, no person shall be subject to any penalty for failing to comply with a collection of information if it does not display a currently valid OMB control number. **PLEASE DO NOT RETURN YOUR FORM TO THE ABOVE ADDRESS.**						
1. REPORT DATE *(DD-MM-YYYY)* October 2020		**2. REPORT TYPE** Technical Report				**3. DATES COVERED (From - To)** April–September 2020
4. TITLE AND SUBTITLE The Potential Impact of Assimilating Satellite-Derived Atmospheric Motion Vectors in Numerical Weather Prediction Modeling for Nowcasting						**5a. CONTRACT NUMBER**
						5b. GRANT NUMBER
						5c. PROGRAM ELEMENT NUMBER
6. AUTHOR(S) Robert E Dumais Jr						**5d. PROJECT NUMBER**
						5e. TASK NUMBER
						5f. WORK UNIT NUMBER
7. PERFORMING ORGANIZATION NAME(S) AND ADDRESS(ES) CCDC Army Research Laboratory ATTN: FCDD-RLC-EM White Sands Missile Range, NM, 88002-5501						**8. PERFORMING ORGANIZATION REPORT NUMBER** ARL-TR-9093
9. SPONSORING/MONITORING AGENCY NAME(S) AND ADDRESS(ES)						**10. SPONSOR/MONITOR'S ACRONYM(S)**
						11. SPONSOR/MONITOR'S REPORT NUMBER(S)
12. DISTRIBUTION/AVAILABILITY STATEMENT Approved for public release; distribution is unlimited.						
13. SUPPLEMENTARY NOTES ORCID ID(s):						
14. ABSTRACT In regions across the globe that do not have readily available conventional weather observation equipment, nontraditional sources such as satellite-derived atmospheric motion vectors (AMVs; which can estimate tropospheric winds) have become of increasing interest. This report provides a short overview of some current literature related to atmospheric motion vectors and their use in numerical weather prediction, along with results from a short study that looks at their potential to influence short-range (up to 3 h) wind forecasts (or "nowcasts") using the US Army Combat Capabilities Development Command Army Research Laboratory's Weather Running Estimate–Nowcast Realtime System, based upon the Advanced Research version of the Weather Research and Forecast model. These observations could prove important to a field artillery Army system like the Profiler Virtual Module, where rapidly updated mesoscale numerical weather prediction model wind forecasts through the troposphere (and even into the stratosphere) provide critical meteorological information for artillery trajectory calculations. Such a system can be deployed anywhere globally. This report explores evidence that AMVs might offer an important alternate source of upper-air wind observations in otherwise data-denied regions of the globe, offering the potential to enhance the accuracy of short-range nowcast predictions in such regions.						
15. SUBJECT TERMS meteorology, nowcasting, modeling, observations, atmospheric motion vector						
16. SECURITY CLASSIFICATION OF:			**17. LIMITATION OF ABSTRACT**	**18. NUMBER OF PAGES**		**19a. NAME OF RESPONSIBLE PERSON** Robert E Dumais Jr
a. REPORT Unclassified	**b. ABSTRACT** Unclassified	**c. THIS PAGE** Unclassified	UU	30		**19b. TELEPHONE NUMBER (Include area code)** (575) 694-5022

Standard Form 298 (Rev. 8/98)
Prescribed by ANSI Std. Z39.18

Contents

List of Figures

List of Tables

1. Introduction

The Profiler Virtual Module (PVM) is a numerical weather prediction (NWP) modeling system fielded by the US Army to generate short-range and frequently updated (i.e., nowcast) meteorological information for making artillery trajectory calculations.

Up until a few years ago, PVM obtained National Oceanic and Atmospheric Administration (NOAA)/National Centers for Environmental Prediction Global Forecast System (GFS) global meteorological model (EMC 2003)[*] forecast data via satellite transmission (Global Broadcast System [GBS]) or over the Internet at a Tactical Operations Center, in addition to World Meteorological Organization observational upper-air sounding and surface data (via GBS). The GFS data were used to initialize the PVM, which executes the Advanced Research version of the Weather Research and Forecasting (WRF-ARW) model (Skamarock et al. 2008). A typical PVM configuration of WRF-ARW is triple-nested to a resolution of 4 km, with 45 terrain-following vertical levels. The system is designed to provide a continuous stream of gridded high-resolution nowcasts by frequently rerunning the nonhydrostatic WRF-ARW with available observations while staying ahead of the clock (Schroeder et al. 2006). Surface, upper-air radiosonde, and aircraft meteorological observations are typically received via the GBS for use in the PVM application of observation nudging four-dimensional data assimilation (FDDA)[†].

During the last couple of years, the PVM has replaced the GFS with the US Air Force 557th Weather Wing's Global Air–Land Weather Exploitation Model (GALWEM) (Stoffler 2017). The GALWEM is the Air Force's own instantiation of the UK's Global Met Office Modeling System[‡].

An issue for the PVM is that in many parts of the globe, conventional weather observation data and equipment of this type are either scarce or altogether absent. However, atmospheric motion vectors (AMVs) are a potential source of supplementary data (Velden et al. 2005) that could be used to fill the void for PVM. AMVs are derived by tracking clouds or areas of water vapor gradients through consecutive satellite images. They have become important sources of tropospheric wind information for NWP, particularly over the oceans and at high latitude where conventional wind data (sondes and aircraft) are scarce (Forsythe and Saunders 2006; Salonen et al. 2015).

[*] https://www.emc.ncep.noaa.gov/users/Eric.Rogers/documents/FV3GFS_OD_Briefs_10-01-18_4-1-2019.pdf
[†] http://www2.mmm.ucar.edu/wrf/users/docs/ObsNudgingGuide.pdf
[‡] https://cpo.noaa.gov/sites/cpo/MAPP/Webinars/2017/09-29-16/Walters.pdf

Both geostationary operational environmental satellites and polar orbiting environmental satellites are used in generating AMVs. A number of international operational centers have developed different algorithms for deriving wind vectors from tracking these atmospheric motions across sequential satellite images. These algorithms are discussed and compared by Santek et al. (2019). In their report, the authors found that the algorithm(s) developed at the Japan Meteorological Agency performed considerably better overall. Other centers that contributed to the study were the Brazilian Center for Weather Prediction and Climate Studies; Korean Meteorological Administration; European Organization for the Exploitation of Meteorological Satellites; NOAA National Environmental Satellite, Data, and Information Service (NESDIS); and the National Weather Center Satellite Application Facility on Support to Nowcasting (NWCSAF). All appeared that they could add value to otherwise data-void areas.

All weather observations inherently contain some amount of error versus the "true" state of the parameter they are attempting to measure. Perhaps the most significant source of error that still exists in the various AMV algorithms has to do with correctly assigning heights/pressures, although these errors appear to be fewer as the algorithms improve over time (Posselt et al. 2019). Recent studies have shown benefits, some substantial, of incorporating AMVs (especially those from the geostationary satellites) into both global and mesoscale NWP operational models. Using the NOAA 3-km High Resolution Rapid Refresh model (based on the WRF-ARW), James and Benjamin (2017) showed a statistically significant (albeit relatively small) improvement in tropospheric wind short-range forecasts from using AMVs and other available sources of observations. However, their study focused mostly upon land over the continental United States. When used in a global modeling system spanning across vast oceanic areas of low data density, Pauley et al.'s study (2016) using the Navy Global Environmental Model (Hogan et al. 2014) showed that the geostationary atmospheric motion vectors had a very strong positive influence on 24-h forecasts.

At NOAA NESDIS, a number of AMV products are generated from both their Geostationary Operational Environmental Satellites (GOESs) and Polar Operational Environmental Satellites using visible (below 675 hPa), IR (175–425 hPa; below 675 hPa), and water vapor (175–475 hPa) channels. In the previous sentence, the parenthesized pressure layers represent where most AMVs from those channels are collected. The GOES products from NOAA NESDIS cover an area of roughly 70° N to 70° S latitude, are available hourly, and are at horizontal resolution of 60 km (although 30-km resolution for the visible channel AMVs).

This report looks briefly at the impact of using NOAA NESDIS hourly geostationary AMVs in FDDA within the WRF-ARW in the Weather Running

Estimate–Nowcast Realtime (WREN_RT) system at the US Army Combat Capabilities Development Command Army Research Laboratory (Reen and Dawson 2018). The WREN_RT can produce short-range nowcasts and is used here to play the role of a surrogate for a potential future higher-resolution version of the PVM. A single case study event from 2016 Apr 28, centered over Yuma Proving Ground (YPG), Arizona, demonstrates the potential benefits.

2. Case Study Event

The case event is from 2016 Apr 28 and is centered over YPG, Arizona. During the period 2016 12 UTC 28 Apr to 00 UTC 29 Apr, a strong upper-level trough and jet streak passage occurred over the southwestern United States and the modeling region of interest. Also during this particular case day, a number of 3-h special radiosonde releases were launched from YPG. This provided an opportunity to examine the impact of using AMVs, with the additional radiosonde data providing a not-so commonly available set of independent ground truths to compare against. Figures 1–3 provide the 12 UTC surface and upper air conditions including the YPG radiosonde site launched just prior to 12 UTC on Apr 28 (Fig. 4). Figure 3 shows that a surface low-pressure center was located near Flagstaff, Arizona, to the east–southeast of the upper low that is over southern Nevada. A surface cold front had already passed through southeast California and southwest Arizona, and was close to entering locations like Phoenix and Ajo, Arizona. A small convective area of shower activity was over southern Nevada close to Las Vegas, with only a scattering of light rain in other locales across southern California. As the upper trough lifted out of the southwestern United States throughout the morning and afternoon of 28 Apr, winds aloft (both in terms of speed and direction) changed considerably over YPG as the associated upper jet streak rotated through. Stale wind observations or model output used for artillery trajectory calculations would be susceptible to significant errors on this day.

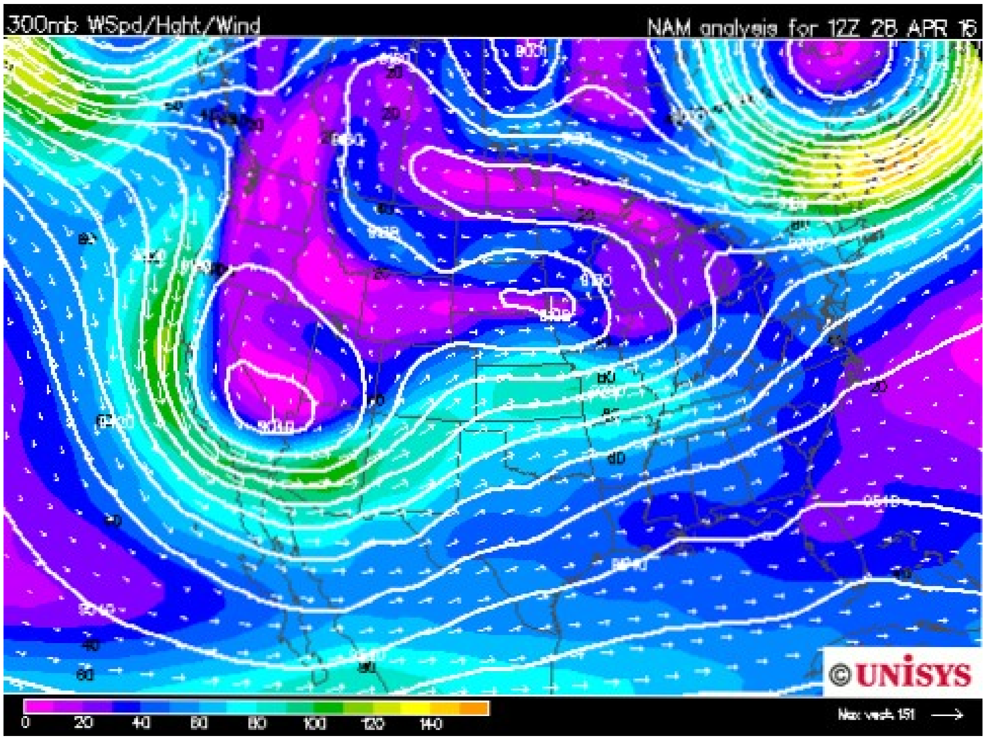

Fig. 1 500-hPa geopotential height and wind analysis valid 12 UTC 28 Apr 2016 (courtesy of Unisys)

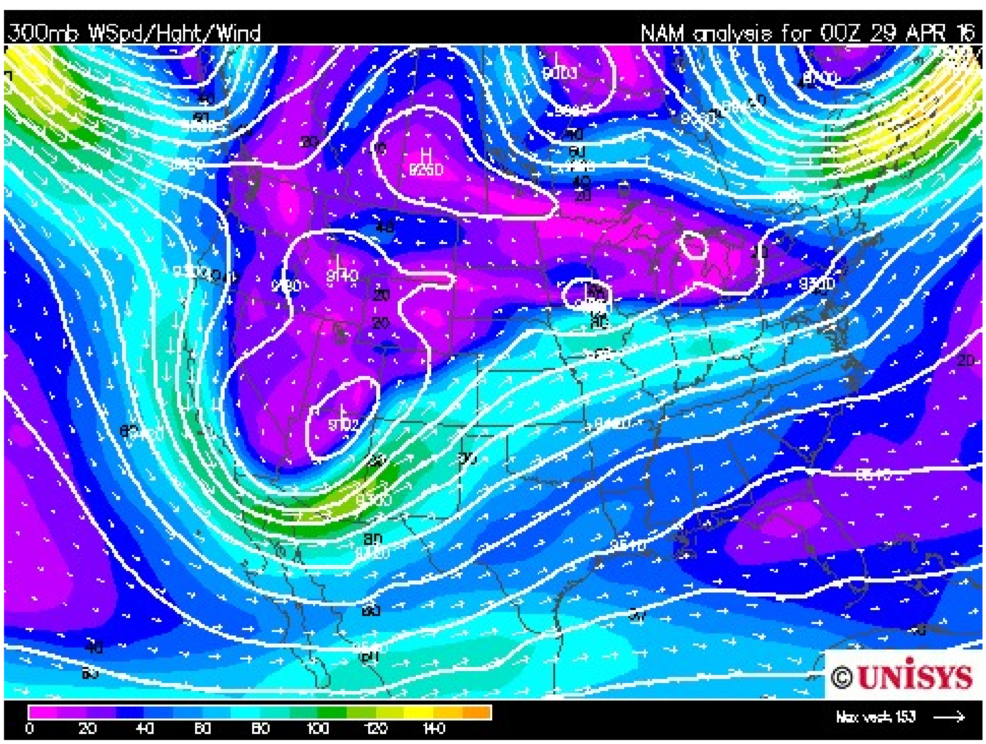

Fig. 2 300-hPa geopotential height and wind analysis valid 12 UTC 28 Apr 2016 (courtesy of Unisys)

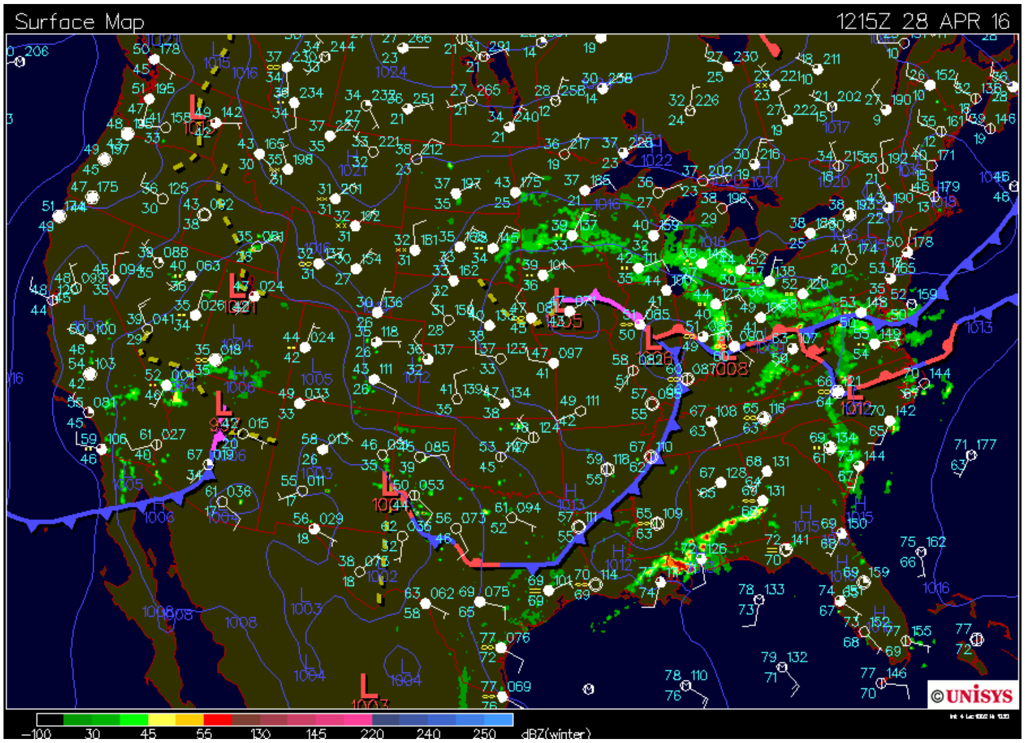

Fig. 3 Surface analysis valid 1215 UTC 28 Apr 2016 (courtesy of Unisys)

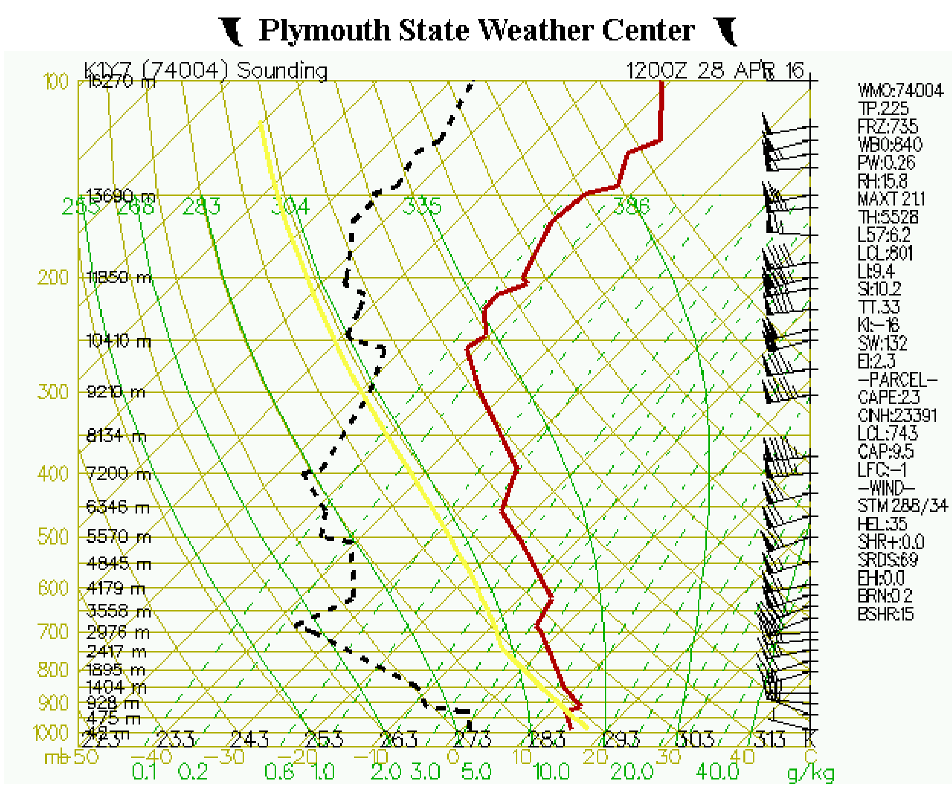

Fig. 4 Yuma Proving Ground (1Y7) radiosonde SkewT-LogP valid 12 UTC 28 Apr 2016 (courtesy of Plymouth State University)

3. WRF-ARW Model Configuration in WREN_RT

For running WREN_RT simulations, the WRF-ARW v.3.9.1.1 used three telescopic nests with the following grid spacing and dimensions: 13.5 km (151 × 151), 4.5 km (151 × 151), 1.5 km (151 × 151). In the vertical, 90 terrain-following levels were used to optimize the spacing of vertical layers with horizontal grid spacing. Using too few levels would invite the possibility that the spacing between certain vertical levels might rival the innermost grid spacing of 1.5 km. To avoid numerical noise in the model, no model vertical layer should exceed some specific ratio compared to the horizontal grid spacing (which gets challenging at grid spacing of about 2 km and finer, so typically more vertical levels are applied when they can be computationally afforded). See, for example, Skamarock et al. (2019).

For first-guess background fields used as initial conditions, and for the time-dependent lateral boundary tendencies along the outer 13.5-km nest, the GFS 1/2 degree forecast model was used (available at 3-h forecast intervals). The GFS forecast cycle used was that from 2016 Apr 28 06 UTC. Throughout the period 12 UTC to 19 UTC on Apr 28, eight WRF-ARW forecast cycles were run at hourly intervals by the WREN_RT for three different experimental configurations to be described later. Each forecast cycle started from a concurrent GFS 1/2 degree initial condition forecast from the 06 UTC cycle, and lateral boundary tendencies for the outer nest were generated similarly through the WRF-ARW preprocessing software used in the WREN_RT. However, forecast cycles for experiments applying data assimilation started at 3 h prior to the start of the desired base time hour to allow for a 3-h period of FDDA to assimilate NOAA Meteorological Assimilation Data Ingest System (MADIS) observations and model spin-up from the coarser GFS initial condition. Each cycle provided 3 h of forecast lead time beyond the desired base time, so for a 12 UTC base time cycle with FDDA, the model would actually run from 09 UTC to 15 UTC (with 09 UTC to 12 UTC being for preforecast FDDA). The WRF-ARW model physics options selected in WREN_RT, as well as other information about the namelist input settings, are listed in Table 1.

Table 1 WRF-ARW model namelist settings and configuration information

Namelist scheme/option	Description	Reference
sf_surface_physics = 2	Noah land surface model	Tewari et al. (2004)
mp_physics = 28	Thompson microphysics	Thompson and Eidhammer (2014)
ra_lw_physics = 4	RRTMG long wave	Iacono et al. (2008)
ra_sw_physics = 4	RRTMG short wave	Iacono et al. (2008)
cu_physics = 3	Grell–Frietas ensemble scale-aware cumulus	Grell and Freitas (2014)
bl_pbl_physics = 5	MYNN PBL	Nakanishi and Niino (2009)
sf_sfclay_physics = 5	MYNN surface layer	Nakanishi and Niino (2009)

Additional model settings	Description
Slope and shading effects on shortwave at surface	Yes (except for 13.5-km outer nest)
2-way nest feedback	Yes
6th order diffusion numerical filter	Yes
Horizontal turbulent diffusion	Smagorinsky 2-D on Cartesian z-surfaces
OBSGRID	Use observations to improve GFS first guess (Cressman analysis used)
OBSGRID	Used also to perform quality control on observations using GFS background field
Expanded domains for observation collection	Used to collect observations across larger domain than nest area during WPS
obs_twindo in namelist	Set to 1.5 h as FDDA observation temporal window (but 75% of this for surface observations)
obs_dtramp in namelist	Set to 60 min and allows model FDDA to gradually ramp down to 0 after the end of FDDA assigned period of 3 h
Observation nudging strength for u and v wind component directions, potential temperature, and water vapor mixing ratio	6.0 × 10-4 s-1
obs_rinxy in namelist	Sets horizontal nudging radii of influence to 120, 60, and 20 km (13.5-, 4.5-, and 1.5-km nests, respectively); reduced by 50% of these for surface variables.
Weight of nudging in vertical	Controlled for surface observations using obs_sfc_scheme_vert=0 for spreading their nudging innovations within the lower boundary layer, but for all other single level observations above the surface, a 75-hPa layer is applied for spreading the observations.
Number of AMVs	Roughly 3000 AMV wind observations available within expanded 13.5-km (nest 1) domain between 11 UTC and 14 UTC.

4. Experiments

The main purpose of this report is to explore evidence that AMVs might offer an important alternate source of upper-air wind observations in otherwise data-denied regions of the globe, offering the potential to enhance the accuracy of short-range nowcast predictions in such regions. The WRF-ARW with FDDA used by WREN_RT in generating the results of this report represents a higher-resolution surrogate for the model and approach used by the PVM system. The AMVs are an additional source of meteorological observations that could be made available to the PVM, since they are collected via the US Air Force 557th Weather Wing. Could the PVM system benefit from the use of these additional (and currently nonused) tropospheric wind observations, since winds are the greatest source of meteorologically generated errors in artillery trajectory calculations?

For each of the eight forecast cycles shown in Fig. 5, three different experimental forecast simulations were run. The first assimilated all NOAA MADIS observations (excluding profilers) into the FDDA (E1), the second assimilated only the AMVs and surface Meteorological Aerodrome Reports (METARs) from MADIS (E2), and the third applied no 3-h assimilation period (E3). For E3, there is no FDDA 3-h preforecast period as shown in Fig. 5. Since this study focuses on just a single case day, and the number of simulations are too few to generate meaningful statistical metrics, this report will focus on a just a small set of qualitative comparisons between the experiments.

09z______12z______15z

10z______13z______16z

11z______14z______17z

12z______15z______18z

13z______16z______19z

14z______17z______20z

15z______18z______21z

16z______19z______22z

Fig. 5 WREN_RT forecast cycles (including 3-h preforecast FDDA period for those experiments that used one)

5. Results

Figures 6 and 7 show vertical profiles (in pressure) of both wind speed (knots; 1 knot = 0.514 m/s) and wind direction (degrees) at a location near the site (32.85° N; –114.4° W) that was releasing radiosondes on YPG (at 3-h intervals) during 2016 Apr 28. The radiosonde release times at YPG were 12, 15, 18, 21, and 00 UTC. These extra YPG radiosondes (including at some asynoptic observing hours) were assimilated into forecast cycles when appropriate within the FDDA window and also used at times as sources of independent model verification (as done in Figs. 6 and 7). The asynoptic radiosondes can be viewed as independent since each model cycle was run independently from its previous cycle (and the asynoptic radiosondes were also not used in the operational GFS cycle used for the initial and lateral boundary conditions).

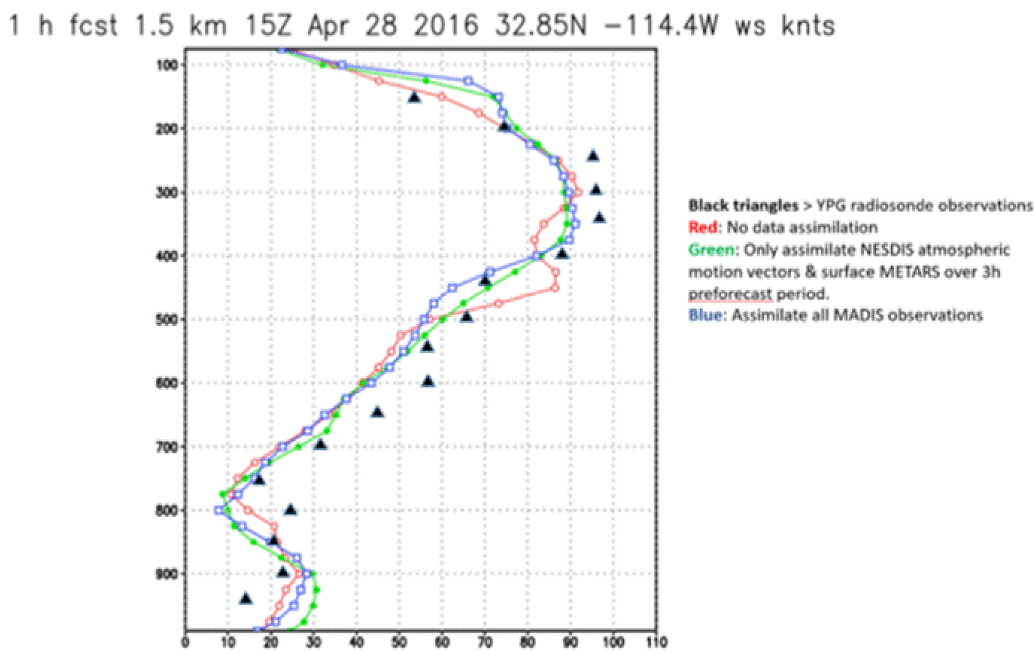

Fig. 6 WREN_RT 1-h forecast (1.5-km nest) valid 15 UTC (from 14 UTC cycle) at YPG 1Y7 radiosonde location, showing wind speed (knots) by vertical pressure level (hPa). 1 knot = 0.514 m/s. Blue curve shows forecast for E1, green for E2, and red for E3. Black triangles are 15 UTC radiosonde observations at 1Y7.

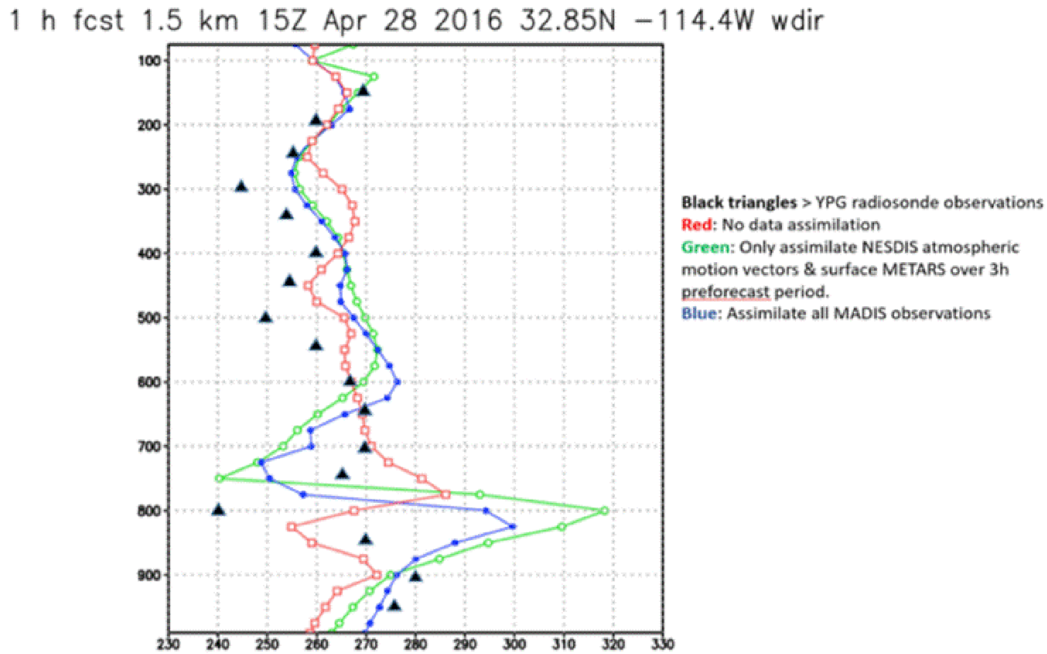

Fig. 7 WREN_RT 1-h forecast (1.5-km nest) valid 15 UTC (from 14 UTC cycle) at YPG 1Y7 radiosonde location, showing wind direction (degrees) by vertical pressure level (hPa). Blue curve shows forecast for E1, green for E2, and red for E3. Black triangles are 15 UTC radiosonde observations at 1Y7.

As can be seen in both Figs. 6 and 7, it is inconclusive from a subjective perspective to determine if the AMVs were particularly helpful (or even detrimental at some levels) to the 1-h wind forecast for this case cycle. The blue curves show 1-h forecasts from the 14 UTC cycle (as vertical profiles in pressure) in the experiment (E1) when all MADIS observations were assimilated (including all 12 UTC radiosondes such as that launched at YPG, which fall within the FDDA period), the green curves show the same but for the experiment E2 when only AMVs from MADIS (i.e., NESDIS) were assimilated, and the red curve shows experiment E3 which used no 3-h preforecast period (and thus no FDDA). The black triangles show observations taken from the special 15 UTC radiosonde at YPG, which is the valid time of the 1-h forecast from the 14 UTC cycle. One can clearly claim that the use of AMVs alone makes a notable difference (in terms of the 1-h wind speed forecast) when compared to the no-data assimilation experiment.

The direction of the changes are usually consistent at most levels when compared to those shown by the blue curves (when radiosondes, AMVs and aircraft observations were all used as sources of upper air data). However, when compared to the black triangles (15 UTC YPG radiosonde observations), it cannot be clearly argued that the changes are always improvements over what was obtained by not using FDDA run (E3). The same can be said of the blue curves (full FDDA) for both wind speed and direction. However, we are making assumptions here that 1) the radiosonde observations represent absolute ground truth in this instance, although this may not necessarily be the case (especially considering that balloon drift is not acounted for in WREN_RT) and 2) that the earlier-mentioned remaining sources of error notable with AMVs have been properly filtered out and quality controled (not likely). In addition, all sources of upper air observations used in the WREN_RT FDDA are assumed to be of the same weight/value, and the user-defined horizontal and vertical radii of influences (Table 1) may not reflect realistic flow-dependent background error covariances. All of that being said, the AMVs do indicate a clear ability to exert influence upon the WREN_RT nowcasts.

Figures 8, 9, and 10 appear to provide additional credence to the idea that the ingest of the AMVs alone was capable of introducing noticeable changes to the 1-h forecasts (again from the 14 UTC cycle). Given the sizable number of AMVs that were available to FDDA (for example, refer to Table 1) during this time period, it is not entirely surprising that they would have some impact. However, the finding is still worthy of acknowledgement, especially as the quality, resolution, and availability of such observations should be expected to continue to improve in the near future. In Figs. 11 and 12, the 0-h nowcast is compared in the 18 UTC cycle (thus valid at 18 UTC) for the three experiments, except to only one another. Similarly, Figs. 13 and 14 show the same 3-h nowcast profiles valid at 21 UTC from the same 18 UTC cycle. Once again, we can note similar findings to what we had previously—that is, no conclusive evidence that these case examples show noticeable overall improvement to the nowcast predictions by the use of AMVs, but certainly suggestions that the AMVs (even in the absence of other types of upper air meteorological observations) can influence the model solutions (most significantly the upper-level wind fields) significantly. Other fields like temperature were also looked at (not shown), but very little impacts (at least subjectively obvious) were noted at the 1-h to 3-h nowcast range. However, all meteorological fields output by the nowcasts will need to be investigated more closely in the future (including precipitation when it is of interest). Since the emphasis in this report related to how AMVs might improve PVM nowcasts for artillery, the focus was mainly on the tropospheric winds.

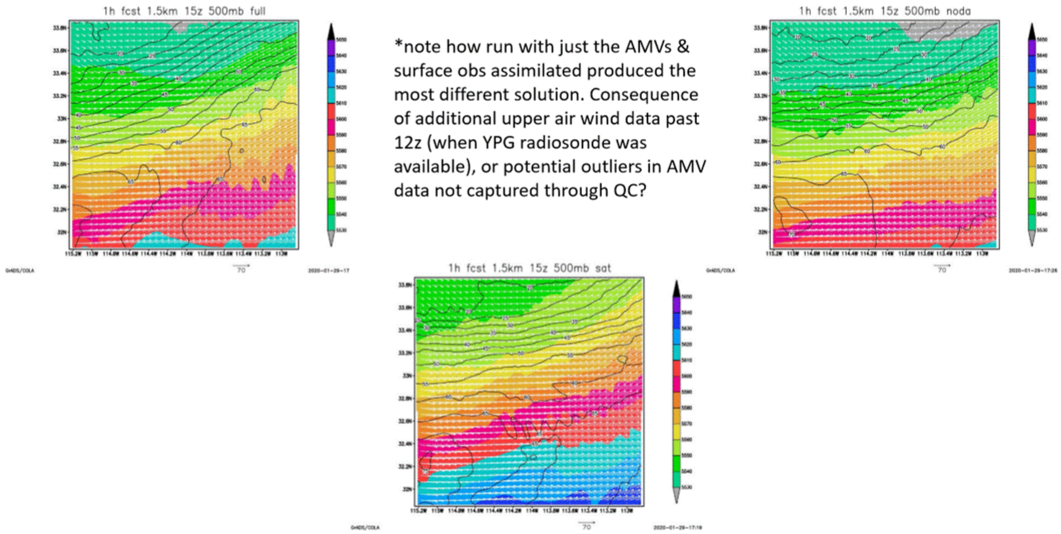

Fig. 8 WREN_RT 1-h forecast (1.5-km nest) valid 15 UTC (from 14 UTC cycle) at 500-hPa pressure level, showing shaded colors of geopotential height (m asl) and contours of wind speed (knots) along with wind vectors

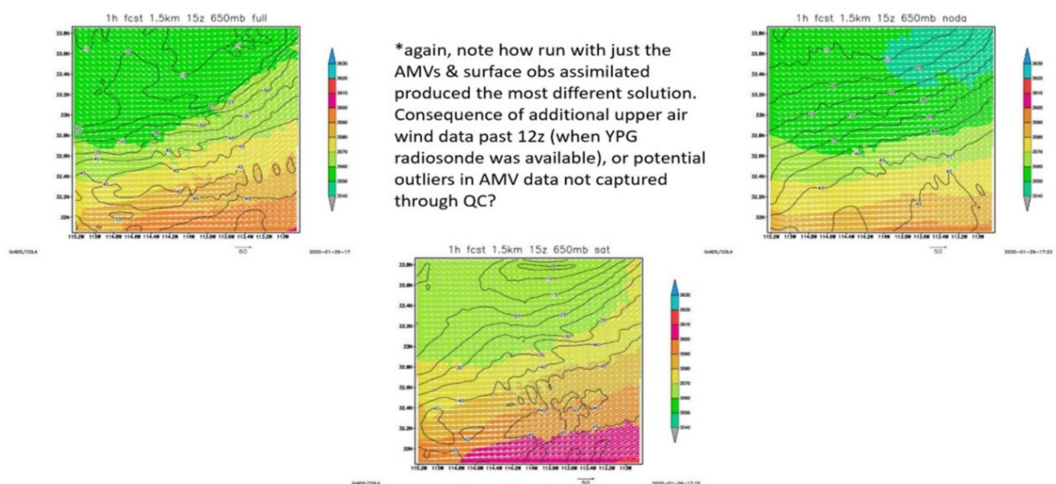

Fig. 9 WREN_RT 1-h forecast (1.5-km nest) valid 15 UTC (from 14 UTC cycle) at 650-hPa pressure level, showing shaded colors of geopotential height (m asl) and contours of wind speed (knots) along with wind vectors

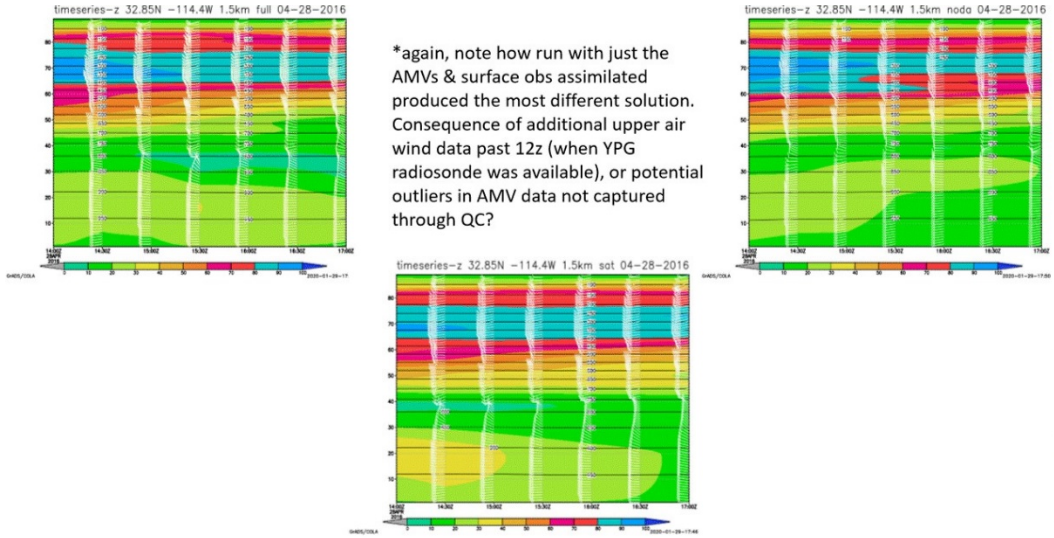

Fig. 10 WREN_RT forecast (1.5-km nest) for grid point nearest to YPG 1N7 radiosonde site, as a time series vertical cross section in height ASL. The shaded colors depict wind speed (knots) and the contour lines show pressure level (hPa).

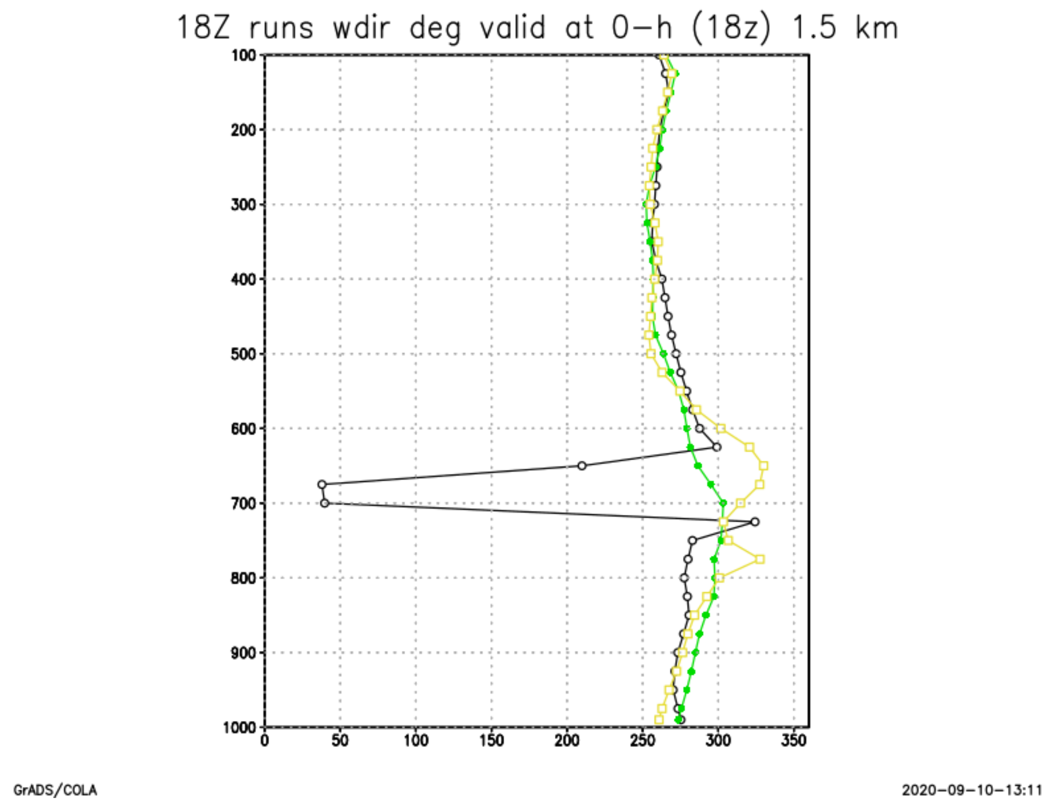

Fig. 11 WREN_RT 0-h forecast (1.5-km nest) at grid point nearest to YPG 1N7 radiosonde site showing wind direction (degrees) with height in pressure (hPa), valid at 18 UTC (produced from 18 UTC cycle). The black curve shows results from E3, the yellow curve from E2, and the green curve from E1.

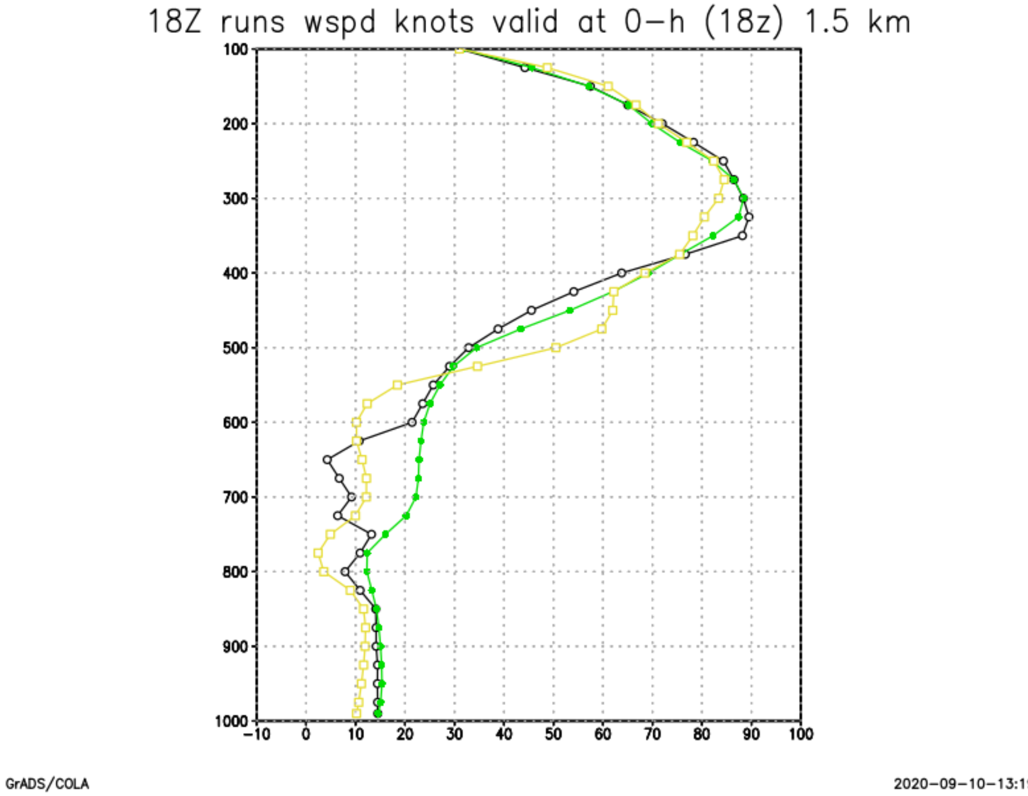

Fig. 12 WREN_RT 0-h forecast (1.5-km nest) at grid point nearest to YPG 1N7 radiosonde site showing wind speed (knots) with height in pressure (hPa), valid at 18 UTC (produced from 18 UTC cycle). The black curve shows results from E3, the yellow curve from E2, and the green curve from E1.

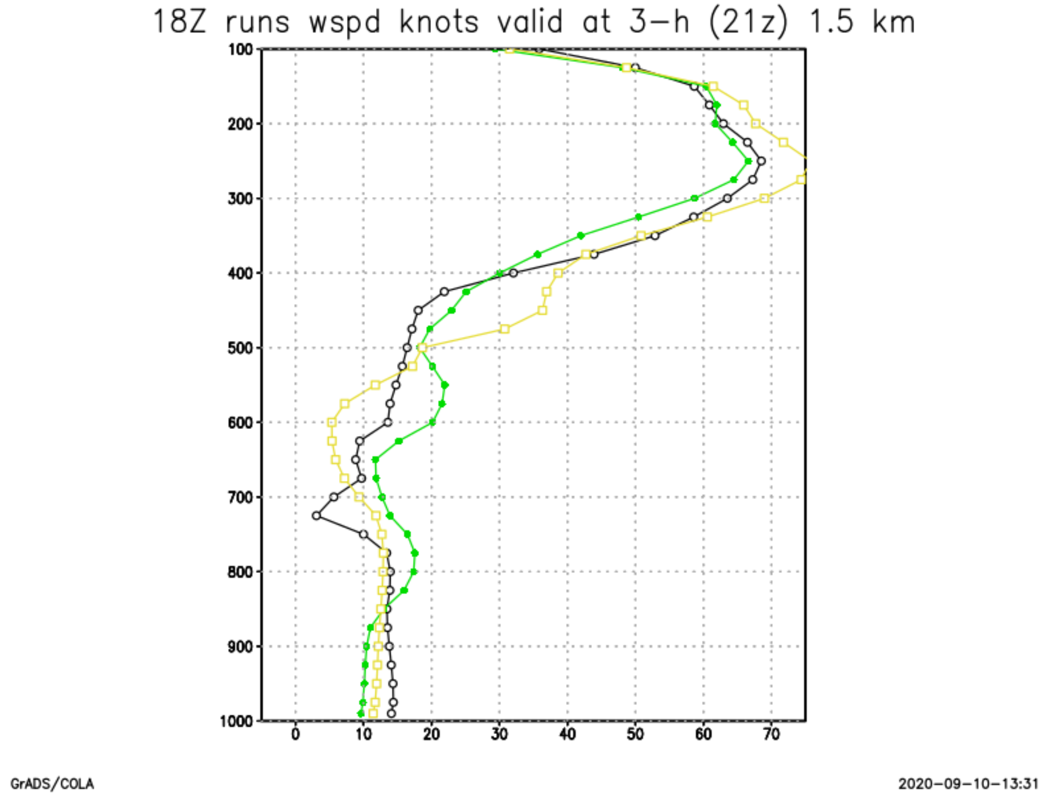

Fig. 13 WREN_RT 3-h forecast (1.5-km nest) at grid point nearest to YPG 1N7 radiosonde site showing wind speed (knots) with height in pressure (hPa), valid at 21 UTC (produced from 18 UTC cycle). The black curve shows results from E3, the yellow curve from E2, and the green curve from E1.

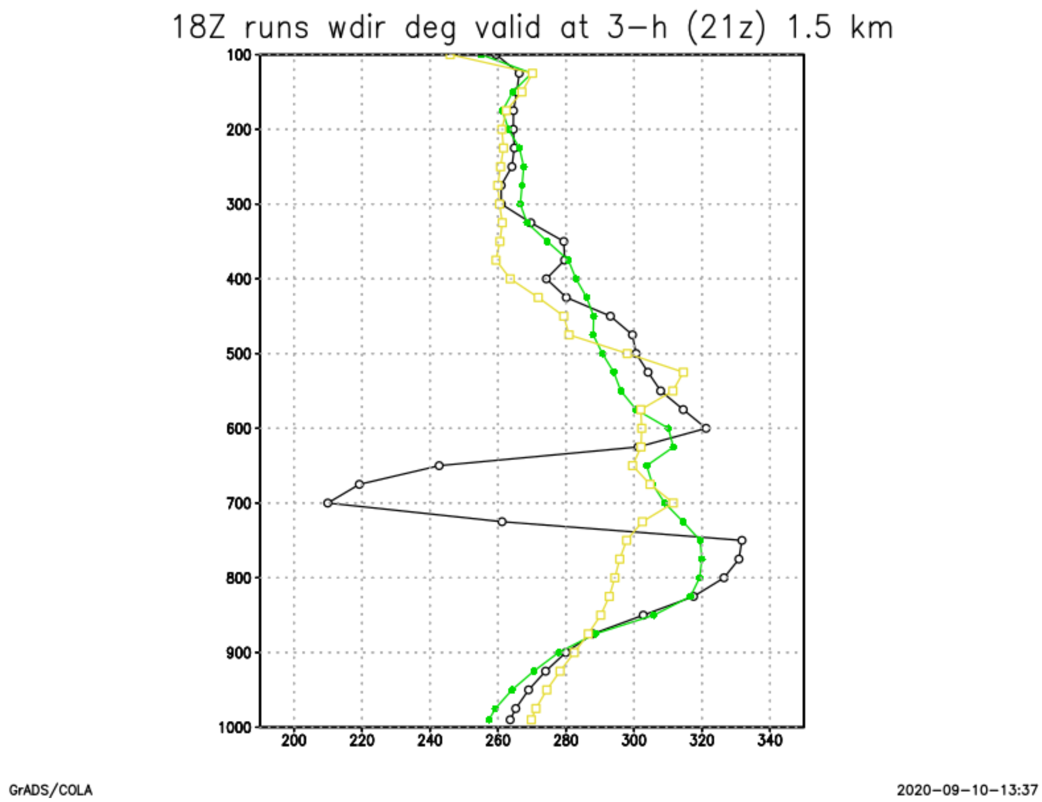

Fig. 14 WREN_RT 3-h forecast (1.5-km nest) at grid point nearest to YPG 1N7 radiosonde site showing wind direction (degrees) with height in pressure (hPa), valid at 21 UTC (produced from 18 UTC cycle). The black curve shows results from E3, the yellow curve from E2, and the green curve from E1.

6. Conclusion

This technical report presented a very short case study that explored the assimilation of AMVs into an NWP-based nowcast system, where AMVs (outside of polar regions) currently offer a satellite-borne alternate source of upper-level tropospheric wind data in regions otherwise data limited (in terms of conventional weather observation sources) as shown in Fig. 15. Specific interest for the Army is associated with NWP-based systems such as the PVM for field artillery, as well as in a potential forward-deployed nowcasting system for the Distributed Common Ground System–Army being tested currently (a scaled-down battalion version of WREN_RT). Although the current field artillery version of PVM is planned to go away in 2023, the same requirements for artillery meteorological support are planned to transfer to the Air Force 557th Weather Wing, either through GALWEM forecasts or possibly a streamlined rapid refresh modeling capability yet to exist (but that has been discussed).

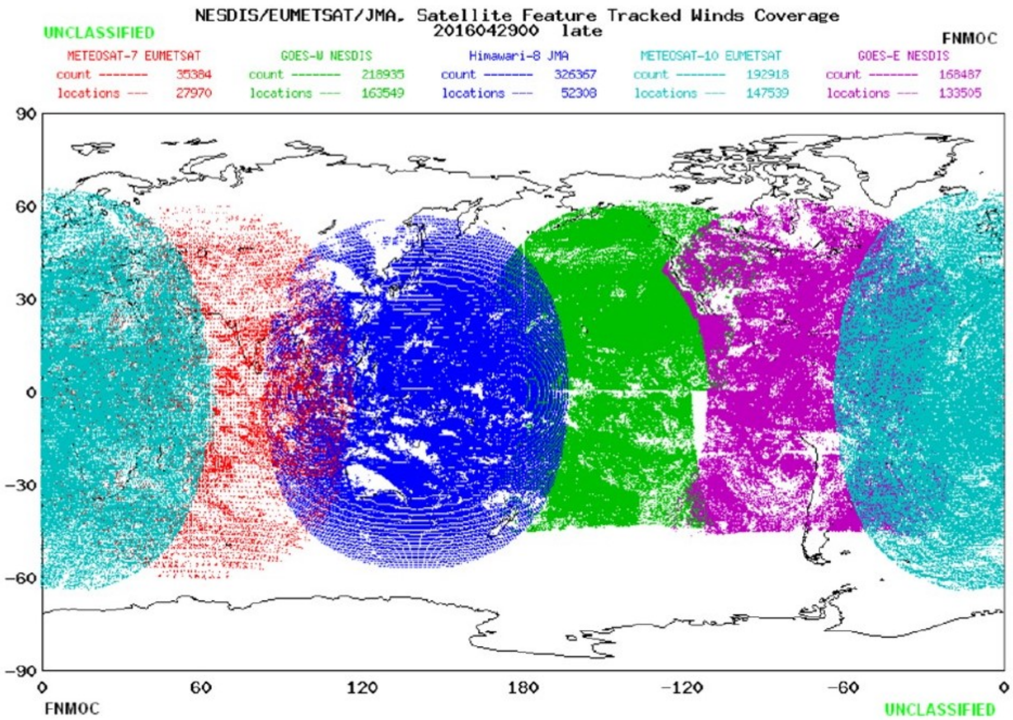

Fig. 15 Typical daily global coverage of AMVs from geostationary satellites (across all major international operational centers) from the day ending 00 UTC 29 April 2016 (courtesy of Naval Research Laboratory's Fleet Numerical Meteorology and Oceanography Center)

The report offered a short history and review of AMVs, including their strengths, areas still in need of improvement, and overall impact via assimilation into current operational NWP modeling at different US and international modeling centers. It then presented results from a brief case study from 2016 Apr 28 across the southwestern United States, which used the WRF-ARW v.3.9.1.1 (the modeling component of the WREN_RT system) to produce a series of hourly 3-h forecasts. The experimental forecasts either assimilated 1) all available meteorological observations (other than profilers) available from the NOAA MADIS, 2) only the AMVs and METAR surface observations as provided by MADIS, or 3) no observations at all. For the two experiments that did assimilate MADIS observations, a 3-h preforecast window was used for FDDA. For the experiment without FDDA, no preforecast window was applied. During the day of the case study, YPG was releasing radiosondes every 3 h to support a field exercise. These were leveraged for both assimilation into the hourly model runs (within the time window of each run's respective FDDA period) and a source of upper-air independent meteorological observations when appropriate.

The wind nowcast results showed the experiment (E1) that used all MADIS observations tended to perform better (i.e., more like the actual nearby radiosonde observations) than the other experiments E2 and E3. However, assuming here that the radiosonde was “perfect” ground truth under such a dynamic and rapidly changing atmospheric flow scenario might be risky due to not accounting for balloon drift in the nowcast FDDA process (Laroche and Sarrazin, 2013). In some examples at specific pressure levels, the results of only assimilating the AMVs seemed to be improved. It is also fair to say that there were a few instances, at a few pressure levels, where the no-FDDA results appeared to be a bit more favorable.

The real benefits that AMVs offered in this study are difficult to quantify for several reasons: limitations in the FDDA and its observation weighting strategy, incomplete quality controlling of outlier AMVs, radiosondes not reflecting absolute ground truth at higher levels aloft (balloon drift), small sample size, and existing WRF-ARW model errors. However, it does seem clear that when used alone in FDDA, they do produce a noticeable effect upon the short-range wind forecasts across all available tropospheric levels. This suggests that in otherwise data-void places around the globe, using AMVs for assimilation short range nowcasts (0–3 h forecasts) much like they have been shown to do for forecasts out to 24 h and even longer. To address winds at levels higher in the stratosphere (above current radiosonde levels) that might impact long-range ballistic trajectories (such as in regions of stratospheric polar jets), different approaches may need to be investigated (Rüfenacht et al. 2012; Borderies et al. 2019). That said, there are probably ample areas of improvement to both the quality control of current AMV data and their assimilation into NWP models like WRF-ARW that would make their use even more advantageous. This will require further and more controlled studies across a much larger sample set.

7. References

Borderies M, Caumont O, Delanoë J, Ducrocq V, Fourrié N, Marquet P. Impact of airborne cloud radar reflectivity data assimilation on kilometre-scale numerical weather prediction analyses and forecasts of heavy precipitation events. Nat Hazards Earth Syst Sci. 2019;19:907–926.

[EMC] Environmental Modeling Center. The GFS atmospheric model. Washington (DC): Department of Commerce (US); 2003 Nov. NCEP Office Note 442.

Forsythe M, Saunders R. Atmospheric motion vectors at the Met office: status, results and future plans. Proceedings of the 8th International Winds Workshop; 2006; Beijing.

Grell GA, Freitas SR. A scale and aerosol aware stochastic convective parameterization for weather and air quality modeling. Atmos Chem Phys. 2014;14:5233–5250.

Hogan TF, Liu M, Ridout JA, Peng MS, Whitcomb TR, Ruston BC, Reynolds CA, Eckermann SD, Moskaitis JR, Baker NL, McCormack JP, Viner KC, McLay JG, Flatau MK, Xu L, Chen C, Chang SW. The Navy global environmental model. Oceanography. 2014;27(3):116–125.

Iacono MJ, Delamere JS, Mlawer EJ, Shephard MW, Clough SA, Collins WD. Radiative forcing by long–lived greenhouse gases: calculations with the AER radiative transfer models. J Geophys Res. 2008;113:D13103.

James EP, Benjamin SG. Observation system experiments with the hourly updating rapid refresh model using GSI hybrid ensemble-variational data assimilation. Mon Weather Rev. Version 1, 2017;145(8):2897–2918.6765

Laroche S, Sarrazin R. Impact of radiosonde balloon drift on numerical weather prediction and verification. Wea Forecasting. 2013;28:772–782.

Nakanishi M, Niino H. Development of an improved turbulence closure model for the atmospheric boundary layer. J Meteor Soc Japan. 2009;87:895–912.

Pauley P, Pauley R, Baker N, Stone R. Overview of satellite-derived winds in NAVGEM. Proceedings for the 13th International Winds Workshop; 27 Jun–1 Jul 2016; Monterey, California.

Posselt DJ, Wu L, Mueller K, Huang L, Irion FW, Brown S, Su H, Santek D, Velden CS. Quantitative assessment of state-dependent atmospheric motion vector uncertainties. J Appl Meteor Climatol. 2019;58:2479–2495.

Reen BP, Dawson LP. The weather running estimate-nowcast realtime (WREN_RT) system, version 1.03. Aberdeen Proving Ground (MD): Army Research Laboratory (US); 2018 Sep. Report No.: ARL-TR-8533.

Rüfenacht R, Kämpfer N, Murk A. First middle-atmospheric zonal wind profile measurements with a new ground-based microwave Doppler-spectro-radiometer. Atmos Meas Tech. 2012;5:2647–2659.

Salonen K, Cotton J, Bormann N, Forsythe M. Characterizing AMV height-assignment error by comparing best-fit pressure statistics from the Met office and ECMWF data assimilation systems. J Appl Meteor Climatol. 2015;54:225–242.

Santek D, Dworak R, Nebuda S, Wanzong S, Borde R, Genkova I, García-Pereda J, Galante Negri R, Carranza M, Nonaka K, Shimoji K, Oh SM, Lee B-I, Chung S-R, Daniels J, Bresky W. Atmospheric motion vector (AMV) intercomparison study. Remote Sens. 2019;11:2240.

Schroeder AJ, Stauffer DR, Seaman NL, Deng A, Gibbs AM, Hunter GK, Young GS. An automated high-resolution rapidly relocatable meteorological nowcasting and prediction system. Mon Wea Rev. 2006;134:1237–1265.

Skamarock WC, Snyder C, Klemp JB, Park S. Vertical resolution requirements in atmospheric simulation. Mon Wea Rev. 2019;147:2641–2656

Skamarock WC, Klemp JB, Dudhia J, Gill DO, Barker D, Duda MG, Huang X-Y, Wang W, Powers JG. A description of the advanced research WRF Version 3. Boulder (CO): University Corporation for Atmospheric Research; 2008. doi:10.5065/D68S4MVH. (No. NCAR/TN-475+STR).

Stoffler RO. The USAF GALWEM: improving military decision making, advancing national capability. 28th Conference on Weather Analysis and Forecasting/24th Conference on Numerical Weather Prediction; 97th American Meteorological Society Annual Meeting; 2017 Jan 22–26; Seattle, WA.

Tewari M, Chen F, Wang W, Dudhia J, LeMone MA, Mitchell K, Ek M, Gayno G, Wegiel J, Cuenca RH. Implementation and verification of the unified NOAH land surface model in the WRF model. 20th Conference on Weather Analysis and Forecasting/16th Conference on Numerical Weather Prediction; 2004; p. 11–15.

Thompson G, Eidhammer T. A study of aerosol impacts on clouds and precipitation development in a large winter cyclone. J Atmos Sci. 2014;71(10):3636–3658.

Velden C, Daniels J, Stettner D, Santek D, Key J, Dunion J, Holmlund K, Dengel G, Bresky W, Menzel P. Recent innovations in deriving tropospheric winds from meteorological satellites. Bull Amer Meteor Soc. 2005;86:205–224.

List of Symbols, Abbreviations, and Acronyms

AMV	Atmospheric Motion Vector
FDDA	Four Dimensional Data Assimilation
GALWEM	Global Air-Land Weather Exploitation Model
GBS	Global Broadcast System
GFS	Global Forecast System
GOES	Geostationary Operational Environmental Satellite
MADIS	Meteorological Assimilation Data Ingest System
METAR	Meteorological Aerodrome Report
MYNN PBL	Mellor–Yamada–Nakanishi–Niino planetary boundary layer
NOAA	National Oceanic and Atmospheric Administration
NWP	Numerical Weather Prediction
PVM	Profiler Virtual Module
RRTMG	Rapid Radiative Transfer Model Global
UTC	Universal Time Coordinate
WREN_RT	Weather Running Estimate–Nowcast Realtime
WRF-ARW	Advanced Research version of the Weather Research and Forecast
YPG	Yuma Proving Ground

1 (PDF)	DEFENSE TECHNICAL INFORMATION CTR DTIC OCA
1 (PDF)	CCDC ARL FCDD RLD DCI TECH LIB
1 (PDF)	CCDC ARL FCDD RLW P R DUMAIS